Appl. Phys. B
DOI 10.1007/s00340-012-5253-9

Applied Physics B
Lasers and Optics

Mode-locked all-fiber ring laser based on broad bandwidth in-fiber acousto-optic modulator

M. Bello-Jiménez · C. Cuadrado-Laborde · A. Diez · J. L. Cruz · M. V. Andrés · A. Rodríguez-Cobos

Received: 2 August 2012 / Revised: 10 October 2012

Abstract Active mode-locking of long-cavity all-fiber ring laser based on broad bandwidth in-fiber acousto-optic modulator (AOM) is reported. The proposed AOM combines the advantages of intermodal coupling induced by standing flexural acoustic waves in a double-ended tapered fiber. We focus our attention on the effects of large tapered transitions to improve the bandwidth modulation. Our approach permits the implementation of broad modulation bandwidth (13 nm), high modulation depth (50 %), and low optical loss (1.1 dB) in an 80-μm configuration. The effects of the AOM in the laser performance are also investigated. Transform-limit optical pulses of 25 ps temporal width and 2.7 W peak power were obtained at 2.46 MHz repetition rate.

M. Bello-Jiménez · C. Cuadrado-Laborde · A. Diez · J. L. Cruz · M. V. Andrés
Departamento de Física Aplicada y Electromagnetismo, ICMUV, Universidad de Valencia, C/Dr. Moliner 50, Burjassot, 46100 Valencia, Spain
e-mail: christian.cuadrado@uv.es

A. Diez
e-mail: antonio.diez@uv.es

J. L. Cruz
e-mail: jose.l.cruz@uv.es

M. V. Andrés
e-mail: miguel.andres@uv.es

M. Bello-Jiménez (✉) · A. Rodríguez-Cobos
Instituto de Investigación en Comunicación Óptica (IICO), Universidad Autónoma de San Luis Potosí, Av. Karakorum 1470 Lomas 4ª Secc., 78210 San Luis Potosí, SLP, Mexico
e-mail: miguel.bello@uv.es; m.bello@cactus.iico.uaslp.mx

A. Rodríguez-Cobos
e-mail: roca@cactus.iico.uaslp.mx

C. Cuadrado-Laborde
CIOp, CONICET, P.O. Box 3, Gonnet, 1897 Buenos Aires, Argentina

1 Introduction

Mode-locked fiber lasers capable of producing ultrashort optical pulses are essential optical sources for a variety of applications in science and technology. For applications in the ultrashort pulse regime passive mode-locking is the preferable technique, but sometimes their poor stability and limited repetition rate becomes a major shortcoming in such schemes. On the contrary, active mode-locking performs a more stable operation, since each optical pulse is triggered by the active mode-locker, which in turn can be accurately synchronized to an external clock signal, and are appropriate for low repetition frequency lasers. The combination of all-fiber and long-cavity configurations should contribute to easy implementation of high-power oscillators. Nevertheless, the main disadvantage associated with active mode-locking is the relatively long pulse generation as a result of the limited electrical bandwidth of the active mode-lockers.

For applications in the ultrashort pulse regime is desired to exploit the full bandwidth available in the host laser medium. Nowadays, in spite of the abundance of scientific information in this field [1–9], new configurations of actively mode-locking operation still can be suggested following the requirements for short or ultrashort pulse generation [5–9]. Among them, all-fiber arrangements are of special interest since they can reduce the intracavity losses associated with coupling to bulk components. Moreover, they provide inherent mechanical stability, and high peak power damage, in addition to compactness and low maintenance requirements. Besides this, and taking

Published online: 22 November 2012

into account the strong influence that dispersion has on the mode-locking process, optical fibers are particularly well suited to form the cavity of a mode-locked laser; cavity dispersion can be easily adjusted just by using fibers with different group velocity dispersions.

In a previous publication we reported an actively mode-locked all-fiber ring laser using a low-insertion loss acousto-optic amplitude modulation technique, which was based on the intermodal coupling induced by standing flexural acoustic waves in a standard optical fiber [7]. In that scheme we found that some limitations exist when the optical bandwidth of the AOM is close to that of the gain medium, limiting the shortest allowable optical pulse in the laser cavity. In this paper, our purpose is to report an improved scheme of the active modulator previously reported in [7]. The proposed AOM combines the advantages of intermodal coupling induced by standing flexural acoustic waves in a double-ended tapered fiber. We focus our attention on the effects of large tapered transitions to improve the bandwidth modulation. Our approach permits the implementation of broad modulation bandwidth (13 nm), high modulation depth (50 %), and low optical loss (1.1 dB) in an 80 μm fiber configuration, operating in the megahertz (MHz) regime. If we compare these results with the previously reported AOM (1.5 nm of optical bandwidth), the optical bandwidth is 8.7 times broader just by reducing the fiber diameter to 80 μm. The total length of the tapered fiber is 23.7 cm long, consisting of 12.5 cm long of taper waist and relatively long (5.6 cm) decaying-exponential profiles. The effectiveness of the AOM is demonstrated by implementing active mode-locking operation in an all-fiber ring laser. Transform-limit optical pulses of 25 ps temporal width and 2.7 W peak power were obtained at 2.46 MHz repetition rate. As compared with our previous result (34 ps chirped pulses and 1.4 W peak power at 4.73 MHz) this represents an important improvement to reach high-quality ultrashort pulse generation at low repetition rates. These experimental results can be considered within the best results reported in the framework of actively mode-locked long-cavity all-fiber lasers.

In the following, we start with an experimental study of the in-fiber acousto-optic modulator, Sect. 2. Then, in Sect. 3 we describe the dependence of the pulse's parameters as a function of the acoustic flexural wave used to drive the AOM. Finally, our conclusions are summarized in Sect. 4.

2 The intermodal coupling acousto-optic modulator with tapered fiber

A schematic view of the acousto-optic modulator (AOM) is shown in Fig. 1. The AOM consists of a RF source, a piezoelectric disk (PD), an aluminum concentrator horn, and a double-ended tapered fiber. We preferred tapering better than etching because, in principle, tapering permits to enhance the acousto-optic interaction by means of two complementary mechanisms. First, tapering increases the acoustic intensity by reducing the cross section of the fiber and, second, it expands the field of the fundamental mode producing an increase of the overlap with both the fields of the optical propagation modes and the acoustic field; consequently, the coupling coefficient is incremented. However, it might be worthwhile to investigate the combination of tapering with etching, since it will provide an extra degree of freedom in the design of the device.

The fiber taper was prepared using a standard fusion and pulling technique, and it was stripped of the outer polymer jacket to prevent the attenuation of the acoustic wave. The total length of the uncoated fiber was 27.5 cm long. The PD is excited by the RF source to produce an acoustic flexural wave that is transmitted to the fiber by the aluminum concentrator horn. The horn is attached to the PD, and it focuses the vibration into the fiber through its tip, which is glued to the uncoated optical fiber. In order to allow the generation of a standing flexural acoustic wave, acoustic reflection is induced by firmly clamping one extreme of the optical fiber, whereas in the other extreme acoustic wave is damped. In our scheme the fiber was tapered down to a fiber diameter of 80 μm, the length of the tapered fiber is 23.7 cm long with relatively long decaying-exponential transition profiles. The tapered fiber was composed of 12.5-cm-long taper waist and 5.6-cm-long exponential transitions.

When a flexural acoustic wave propagates along an optical fiber, it produces a periodical perturbation of the refractive index at the acoustic wavelength Λ, which, in combination with the optical field, can be used to produce intermodal coupling between the fundamental core mode and some specific cladding modes [10–12]. This acousto-optic interaction can be seen as an acoustically induced long period fiber grating (LPG) whose transmission properties can be controlled dynamically by varying the characteristics of the flexural acoustic wave. The optical

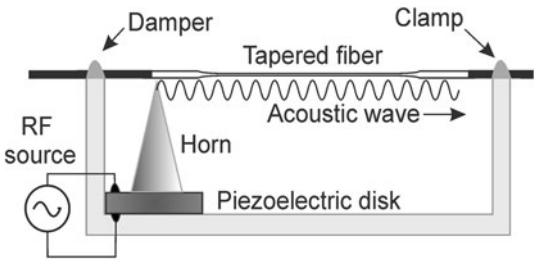

Fig. 1 Experimental setup of the acousto-optic modulator with double-ended tapered fiber

coupling is resonant in wavelength and it takes place at the optical wavelength that verifies the phase-matching condition [11, 12]. At the output, only the light that remains guided by the core mode is transmitted, and the coupling between the fundamental core mode to one of the cladding modes results in the appearance of an attenuation notch in the spectrum at the resonant optical wavelength λ_R, whose amplitude and spectral location remains fixed whenever a traveling acoustic wave is used.

In resonance, λ_R is directly proportional to the root square of the fiber radius R, expressed by the following relation

$$\lambda_R = (n_{co} - n_{cl})\sqrt{\frac{\pi C_{ext} R}{f_a}}, \quad (1)$$

where n_{co} and n_{cl} represents the effective indexes of the fundamental core mode and the cladding mode, respectively. C_{ext} is the speed of the extensional wave, 5760 ms^{-1} for silica, and f_a is the acoustic wave frequency. From this expression can be observed that a small variation in R can be used to produce a shift in the resonant wavelength, since λ_R has an explicit dependence on R and also an implicit dependence through n_{co} and n_{cl}. Hence, by imposing a gradual reduction of the fiber diameter, via the taper transition, a gradual shift of the resonant wavelength that will contribute to enrich the spectral response of the acoustically induced LPG is expected. In addition, the gradual confinement of the acoustic wave also leads to a strong acousto-optic interaction, which results in a more efficient intermodal coupling [13, 14]. Figure 2 shows the transmission spectra of the acoustically induced tapered LPG. As a manner of comparison, and to show the improvement in the spectral response, Fig. 2 includes the transmission spectra for a non-tapered standard optical fiber. In these particular cases the acoustic frequency was selected to produce the maximum transfer of energy at a resonant wavelength around 1,530 nm, the acoustic frequency was fixed at 1.23 and 2.49 MHz for the tapered and non-tapered fiber, respectively.

The spectral response of the tapered fiber reveals a −3 dB optical bandwidth of 11.68 nm with a minimum transmittance of −16 dB at the optical resonant wavelength of 1,531.2 nm. If we compare the values with the spectral response of the non-tapered fiber (−12 dB of attenuation and 1.5 nm of optical bandwidth), then we can appreciate the improvement achieved with the present scheme. Numerical simulations reveal that spectral broadening can be attributed to the combined spectral responses of the taper transitions and the uniform taper waist. For illustration Fig. 3 shows numerical simulations of the transmission spectra for the taper transition, the taper waist, and the total tapered fiber, considering each section as independent in the tapered structure.

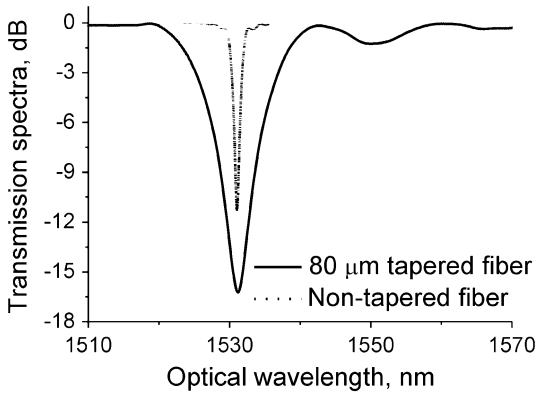

Fig. 2 Transmission spectra for an acoustically induced LPG consisting of an 80 μm double-ended tapered fiber (*solid line*). The *dotted line* represents the transmission spectra for a non-tapered standard optical fiber. The acoustic frequencies were fixed to 1.23 and 2.49 MHz, respectively, to obtain optical resonances around 1,530 nm

For this particular case, it can be observed from Fig. 3 that the resonant wavelength is fixed by the taper waist, whereas the effect of the taper transition can be understood as the improvement in the coupling efficiency that leads into a depth attenuation notch and a broad spectral response. The period of the acoustically induced LPG is estimated to be 767.12 μm in the taper waist, obtained from the dispersion relation for a flexural wave on a cylindrical rod $\Lambda = (\pi R C_{ext} f_a^{-1})^{1/2}$ [11].

The spectral transmission as a function of the acoustic wave is shown in the Fig. 4. When the acoustic frequency changes, the periodicity of the perturbation also varies, therefore the phase-matching condition is shifted to a different resonant wavelength. Figure 4a illustrates the shift of the optical resonant wavelength as a function of the acoustic frequency. These transmission spectra were measured using a broadband light source and an optical spectrum analyzer (OSA) with 50 pm resolution. The three spectra reported in Fig. 4a correspond to three different acoustic frequencies which give rise to a transmission dip at different optical resonant wavelengths. According to the phase-matching condition, the resonant wavelength shifts to shorter wavelengths as the acoustic frequency increases. The inset of Fig. 4a shows a linear dependence of the resonant wavelength with the acoustic frequency f_a. The rate of change was measured to be −1.285 nm/kHz. Figure 4a also shows that the transmission dips have different depths as a function of f_a. This feature is quite common in this kind of acousto-optic devices and its origin is the non-flat frequency response of the PD. For the specific device of our experiments, the highest mode-coupling was found to be around an optical wavelength of 1,530 nm. Thus, in order to obtain the maximal mode-coupling, and consequently the highest modulation depth, the AOM is operated

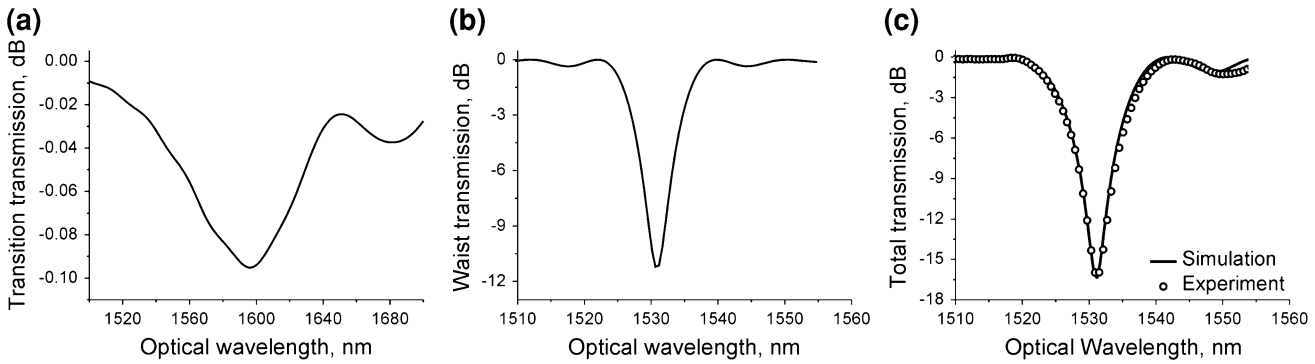

Fig. 3 Numerical simulations of the transmission spectra: **a** taper transition, **b** taper waist, and **c** total tapered fiber. *Open circled* in **c** represents the experimental results

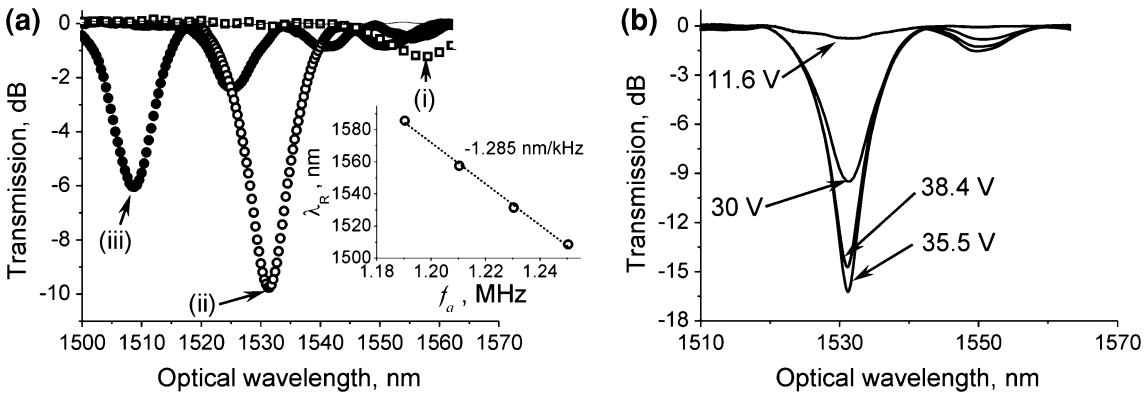

Fig. 4 **a** Transmission spectra at constant RF voltage (30 V) and three different acoustic frequencies: (*i*) 1.2103 MHz, (*ii*) 1.2303 MHz, and (*iii*) 1.2503 MHz. The *inset* gives the calibration of the device: resonant wavelength versus acoustic frequency. **b** Transmission spectra at constant acoustic frequency (1.2303 MHz) and different RF voltages (see the label of each trace)

near this optical wavelength. On the other hand, we analyzed the operation of the AOM as a function of the RF voltage applied to the PD. Figure 4b shows the transmission spectra of the AOM at a fixed acoustic frequency and for different voltages applied to the PD, V_{PD}. For this set of measurements the applied voltage was varied in a range between 11.6 and 38.4 V (whenever we refer to voltages, it is a peak-to-peak measurement), and the acoustic frequency was fixed at 1.2303 MHz. As it can be observed, for low voltages the coupling, and the transfer of power, between the core and the cladding mode increase, resulting in a maximal attenuation notch at 35.5 V. Beyond this voltage the depth of the transmission dip reduces gradually since the two modes are overcoupled and the net transfer of power is reduced. In addition, the response of the PD degrades for high voltage values due to an excessive heating. Most of our experiments were carried out using voltages around 30 V, where a stable and linear response of the PD was observed.

An important characteristic of the acoustically induced LPG occurs when acoustic reflection is induced; the device exhibits a transmission which oscillates in time as a result of the formation of a standing flexural wave. Hence, the transmission is amplitude modulated at a frequency two times the frequency of the acoustic wave. Figure 5a shows the wavelength dependence of the maximum and minimum transmittance for a RF signal applied to the piezoelectric disk of 1.2321 MHz and 14.2 V. The spectral response reveals a minimum transmittance of −8 dB at the resonant wavelength of 1,531.5 nm. At this wavelength the coupling between optical modes produces the maximum transfer of energy and consequently the maximum amplitude modulation. Figure 5b shows the transmitted light as a function of time at the resonant optical wavelength, for the same conditions described in Fig. 5a. It can be clearly observed an amplitude modulation at 2.4642 MHz, which is two times the acoustic frequency used (1.2321 MHz). The measurements reported in Fig. 5 were performed by illuminating the AOM with a laser tuned to a wavelength around the optical resonant wavelength and detecting the transmitted light in a standard oscilloscope. The fact that the reflection coefficient for the acoustic wave is not 1 makes the maximum transmission to be slightly below the reference level, i.e., the transmission of the fiber when no

acoustic wave propagates. Therefore, the maximum transmission determines the insertion loss of the AOM at a given wavelength, RF frequency, and voltage. The difference between the maximum transmission and the minimum determines the modulation depth. From the results presented in Fig. 5, we can emphasize that a strong modulation depth (50 %) is achieved, together with a low-insertion loss (1.1 dB) and a broad operation bandwidth (13 nm). If we compare the optical bandwidth with the values recently reported for an AOM based on a non-tapered AOM [7] (1.5 nm bandwidth), we can appreciate the improvement achieved just by a small amount of reduction in the fiber diameter with the present AOM.

For applications, the modulator has a number of specific characteristics that require to be properly analyzed. First, we measured the modulation depth as a function of the optical wavelength, when both the acoustic frequency and the RF voltage were fixed. The intermodal coupling exhibits a broad bandwidth around the resonant wavelength that satisfies the phase-matching condition. Figure 6a shows the modulation dependence around the resonant wavelength of 1531.5 nm when $f_a = 1.2321$ MHz and $V_{PD} = 14.2$ V. At the resonant wavelength the modulation depth is maximal, and symmetrically decreases for longer and shorter wavelengths. The measured full width at half maximum (FWHM) of the AOM is 13 nm, with a maximum modulation depth of 50 %. On the other hand, since an acoustic resonator is also formed, Fig. 6b shows the modulation depth versus the detuning frequency) f_a when λ_R and V_{PD} are fixed at 1,531.5 nm and $V_{PD} = 14.2$ V, respectively. The center frequency in Fig. 6b corresponds to 1.2321 MHz; at this frequency the modulation depth is maximal, and it drops gradually to values near to zero for frequencies of around ±1 kHz. For longer and shorter frequencies the transmission periodically oscillates and decays gradually with periodicity of about 3.7 kHz.

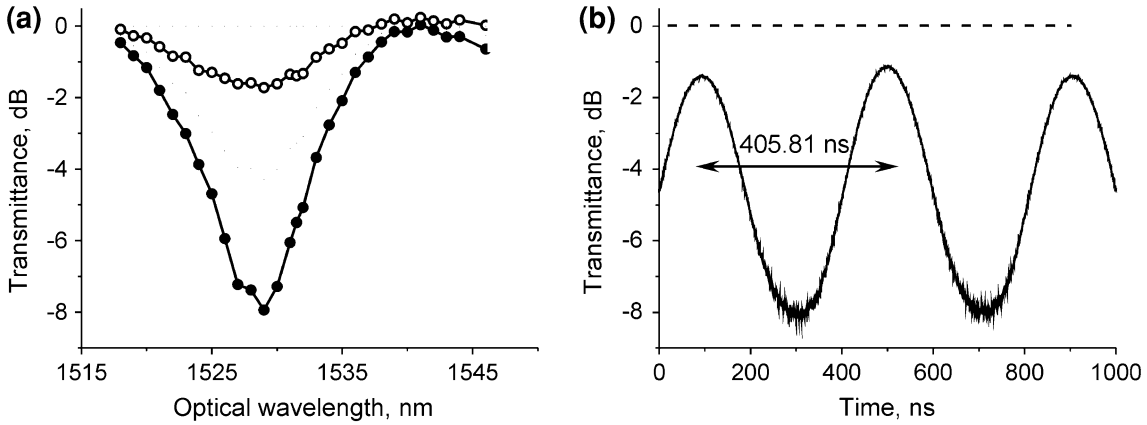

Fig. 5 **a** Maximum (*solid points*) and minimum (*open points*) transmittance of the AOM as a function of wavelength, around the resonance located at 1,531.5 nm. **b** Oscilloscope trace that corresponds to the transmission of the AOM (*solid curve*) recorded at the resonant wavelength; the reference level is the *dashed line*. In both cases $f_a = 1.2321$ MHz and $V_{PD} = 14.2$ V

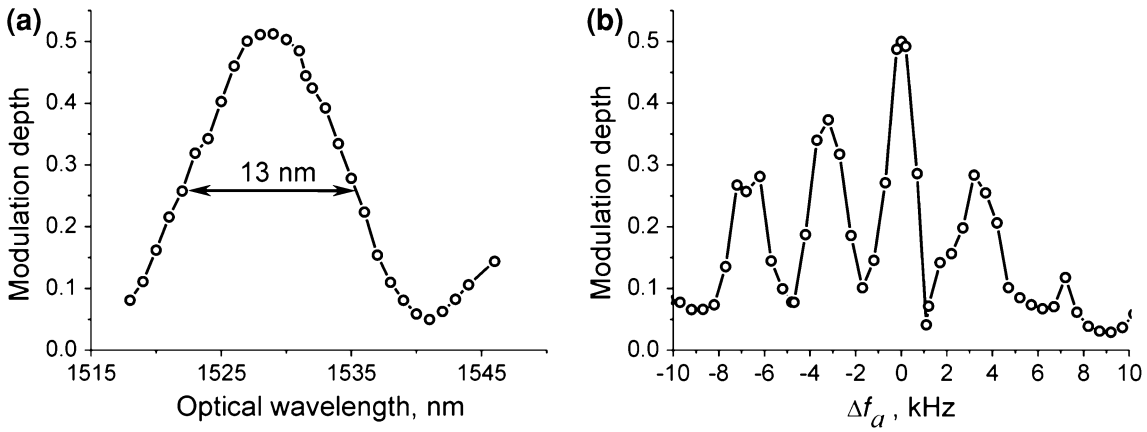

Fig. 6 **a** Modulation depth as a function of the optical wavelength at constant acoustic frequency (1.2321 MHz) and RF voltage (14.2 V). **b** Modulation depth as a function of the detuning frequency (f_a) when both the resonant optical wavelength (1,531.5 nm) and the RF voltage (14.2 V) are fixed. The central acoustic frequency in Fig. 6**b** is 1.2321 MHz

Therefore, the proper operation of the AOM is determined by the acoustic frequency f_a, which is selected to achieve the maximum modulation depth.

From the point of view of the implementation, the AOM is well suited for active mode-locking in the ultrashort pulse regime. The AOM can be operated with a modulation depth of 0.5 in the optical wavelength region of 1,530 nm with a broad modulation bandwidth (13 nm). Moreover, since the AOM can be dynamically controlled by the acoustic wave; fine-tuning of the acoustic frequency will permit a precise matching of the cavity round-trip time with the modulation period. In the next section, we describe the operation of the AOM to perform active mode-locking.

3 Laser setup and results

A schematic diagram of the mode-locked fiber ring laser is illustrated in the Fig. 7. The medium gain was provided by 1.12 m of an erbium-doped fiber (EDF) containing 300 ppm Er^{3+}. The EDF was pumped through a wavelength division multiplexer coupler (WDM) by a 976-nm pigtailed laser diode, providing a maximum pump power of 600 mW. Next, and following the clockwise sense, it was inserted the AOM, followed by a symmetrical optical coupler. One output port of the fiber coupler is used to provide the output light pulses, whereas the remaining port is connected to a delay line; this delay line was necessary in order to match the round-trip time with the modulation period. Then, port 1 of a polarization-independent three-port optical circulator (OC) was connected to the end of the delay line. The OC was used to force unidirectional operation within the ring cavity and to incorporate, via port 2, a fiber Bragg grating (FBG) as a spectral filter. The inclusion of a spectral filter was necessary in order to prevent laser emission at different optical wavelengths of the EDF

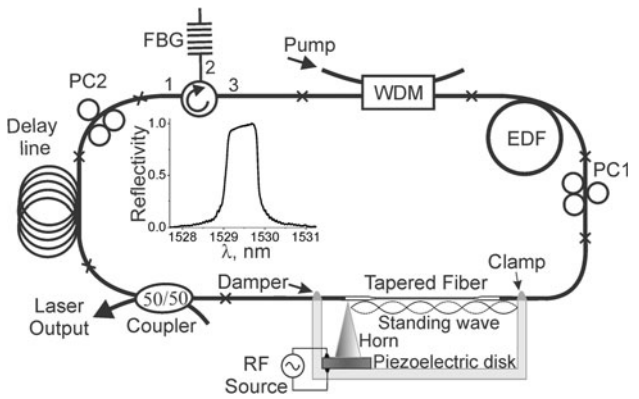

Fig. 7 Schematic setup of the mode-locked fiber ring laser. The *inset* is the reflection spectrum of the FBG

spectrum. The FBG had a Bragg wavelength of 1,529.5 nm, with nearly flat reflectivity of 100 %, and a FWHM bandwidth of 0.7 nm. Finally, the ring cavity was closed by connecting port 3 of the OC to the WDM. Two polarization controllers PC1 and PC2 were added within the cavity in order to allow a fine adjustment of the polarization.

The acoustic frequency f_a was selected to be the same as in Fig. 6a (1.2321 MHz). Assuming an effective index (n_{eff}) of 1.4463 the required cavity length, $L_{cavity} = c/(n_{eff}2f_a)$, is calculated to be 84.18 m. The small errors in cavity length are compensated by a fine adjustment of the acoustic frequency at the rate −6.83 cm/kHz ($\partial L_{cavity}/\partial f_a = -L_{cavity}/f_a$). Since any change of f_a produces a shift of the optical resonant wavelength, the Bragg wavelength of the FBG needs to be shifted to match the optical resonant wavelength of the AOM. For that reason, the FBG is mounted on a translation stage to provide wavelength tuning in a range between 1,529.5 and 1,532.5 nm. This allows a precise matching of the laser wavelength with the resonant wavelength of the AOM.

Regarding the cavity dispersion, we measured the fiber dispersions in the cavity by the frequency-domain modulated-carrier method. The cavity consist of a mixed-dispersion fiber ring with 1.12 m of EDF with $D = -18.8$ ps/(nm km), 5.56 m of SMF-28 with $D = 15.6$ ps/(nm km), 48.99 m of Corning LEAF fiber with $D = 2$ ps/(nm km), 27.34 m of Fibercore SM980 fiber with $D = -5.7$ ps/(nm km), and 1.17 m of OFS 980 fiber with $D = -3.53$ ps/(nm km). The dispersion of the FBG, being a uniform grating, is assumed to be negligible around the Bragg wavelength. Thus, the cavity dispersion results in a zero dispersion cavity with average dispersion (D_{avg}) of 0.044 ps/(nm km).

Mode-locking operation was obtained at the modulation frequency of 2.4616904 MHz and the optical wavelength of 1,529.8 nm. The RF signal used to drive the piezoelectric transducer together with the train of mode-locked pulses is shown in Fig. 8a. As it can be observed, the frequency of the optical pulse train is the double of the frequency of the signal used to drive the PD in the modulator (2.4616904 MHz). Figure 8b shows the dependence of the pulse's parameters as the pump power is varied. Mode-locking operation was found in a range between 172 and 195 mW of pump power. The pulse width monotonically decreases, whereas the peak power increases with the pump power; at the highest pump power, pulses as short as 26.3 ps were obtained with a peak power of 2.7 W.

The dependence of the pulse's parameters with the modulation depth, via the applied voltage to the piezoelectric disk, is shown in Fig. 9a. In this case, the polarization adjustment and the frequency value were kept constant throughout the measurements. The range of

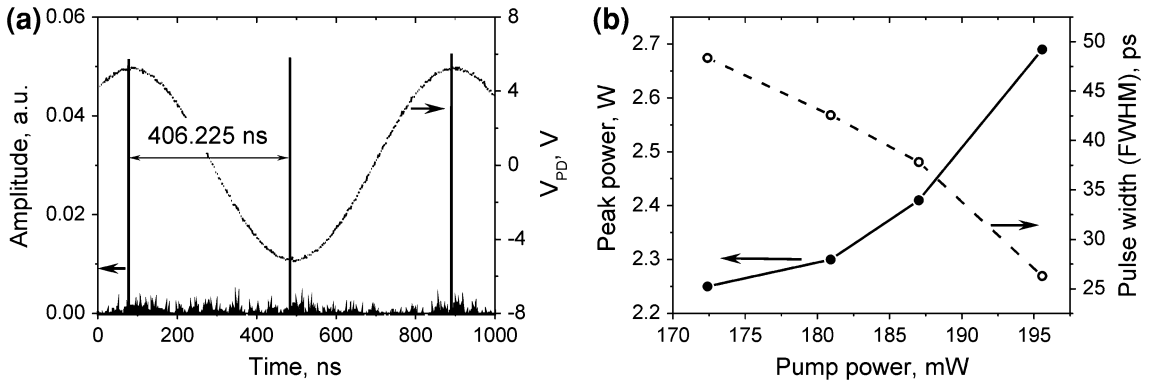

Fig. 8 **a** RF voltage used to drive the PD and mode-locked train of pulses generated at 2.4616904 MHz with 195 mW of pump power. **b** Pulse width (FWHM) and peak power of the optical pulses as a function of the pump power (*open and solid scatter points*, respectively)

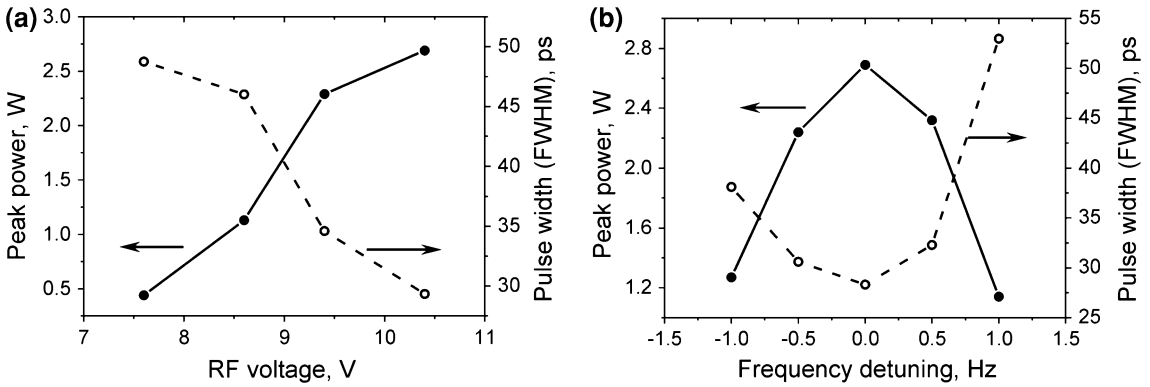

Fig. 9 **a** Pulse width (FWHM) and peak powers versus RF voltage at $f_a = 1.2308372$ MHz (*open and solid scatter points*, respectively). The pump power was 195 mW. **b** Peak power and pulse width as a function of the frequency detuning

voltages which sustains mode-locking was found between 7.6 and 10.4 V. It can be observed in Fig. 9a the narrowing of the output light pulses as the voltage increases, from 49 ps at 7.6 V up to 29 ps for an applied voltage of 10.4 V. In this range, the modulation depth increases with the applied voltage. According to mode-locking theory, the modulation depth and the pulse width are inverse parameters [15, 16]. In this sense, this narrowing is an expected behavior.

Another important parameter to quantify is the maximum allowable frequency detuning (Δv), the maximum difference between the reciprocal of the cavity round-trip time and the modulation frequency that sustains mode-locking. Figure 9b shows the variation of the pulse's parameters as the frequency of the RF signal applied to the PD is changed, while the polarization adjustment and V_{PD} were kept constant. Mode-locking of this laser permits a maximum detuning of about ± 1 Hz in any direction. According to theory of detuning in AM mode-locking, the maximum allowable detuning is inversely proportional to the modulator optical bandwidth, in this case imposed by the FBG bandwidth [15, 16]. This last result implies that frequency detuning becomes an important parameter as the mode-locked pulses become narrower. Consequently, high accuracy in frequency tuning is necessary to implement active mode-locking in the ultrashort pulse regime.

Figure 10 shows the shortest pulse obtained with this configuration and the measured optical spectrum of the laser. The measured temporal width was 25.35 ps (FWHM), with a maximum peak power of 2.67 W and a repetition rate of 2.4616904 MHz. For this pulse the spectral linewidth was measured to be 0.14 nm using a 50-pm resolution optical spectrum analyzer. The time-bandwidth product for the shortest pulse was 0.3145, which corresponds to the transform-limit value of 0.315 for a $\mathrm{Sech}^2(x)$ pulse. From the comparison between these last values, we can conclude that the optical pulses of our mode-locked laser are transform-limit.

As it can be observed, the spectral linewidth of the laser is rather shorter than the 0.7 nm bandwidth of the FBG. In this respect, we believe that due to the group delay dispersion of the FBG, which becomes large in their extreme wings, severe limitations are induced limiting the laser linewidth. As a consequence, further narrowing by this

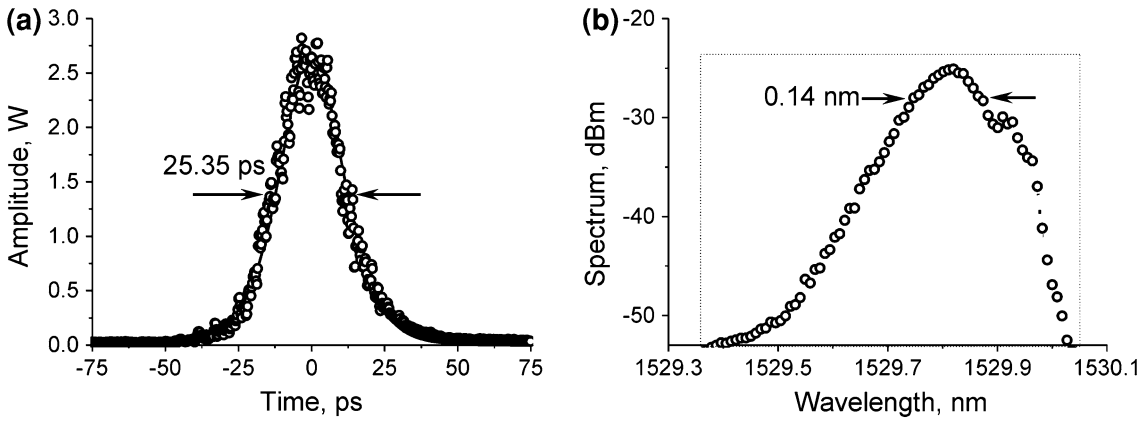

Fig. 10 **a** Oscilloscope trace of a single mode-locked pulse at 2.4616904 MHz repetition frequency. **b** Measured optical spectrum of the laser

trend is theoretically possible, but experimentally challenging, because of the difficulties associated with the fabrication of a broad bandwidth spectral filters without chirp and fine-tuning of the modulation frequency.

4 Conclusions

Actively mode-locking in an all-fiber ring laser was demonstrated using a broad bandwidth in-fiber acousto-optic modulation. The proposed AOM combines the advantages of intermodal coupling induced by standing flexural acoustic waves in a double-ended tapered fiber. Our approach permits the implementation of broad modulation bandwidth (13 nm), high modulation depth (50 %), and low optical loss (1.1 dB) in an 80-μm modulator configuration. The effectiveness of the AOM is demonstrated by implementing active mode-locking operation. Transform-limit optical pulses of 25 ps temporal width and 2.7 W peak power were obtained at 2.4616904 MHz repetition rate. These experimental results can be considered within the best results reported in the framework of actively mode-locked long-cavity all-fiber lasers.

Acknowledgments This work has been financially supported by the *Ministerio de Educación y Ciencia and the Generalitat Valenciana of Spain* (projects TEC2008-05490 and PROMETEO/2009/077, respectively). M. Bello-Jiménez was supported by *CONACyT* (Mexican Council for Science and Technology). C. Cuadrado-Laborde acknowledges the *Programa de Investigadores Invitados de la Universidad de Valencia* (*Spain*). A. Rodríguez-Cobos acknowledges partial support from *C12-FAI-03-83.83*.

References

1. M.W. Phillips, A.I. Ferguson, G.S. Kino, D.B. Patterson, Opt. Lett. **14**, 680 (1989)
2. D.O. Culverhouse, D.J. Richardson, T.A. Birks, P.St.J Russell, Opt. Lett. **20**, 2381 (1995)
3. R.P. Scott, C.V. Bennett, B.H. Kolner, Appl. Opt. **36**, 5908 (1997)
4. M. Jeon, H.K. Lee, K.H. Kim, E. Lee, W. Oh, B.Y. Kim, H. Lee, Y.W. Koh et al., Opt. Commun. **149**, 312 (1998)
5. M. Fabert, V. Kermène, A. Desfargues-Berthelemot, P. Blondy, A. Crunteanu, Opt. Lett. **12**, 2191 (2012)
6. M. Malmström, W. Margulis, O. Tarasenko, V. Pasiskevicius, F. Laurell, Opt. Express **20**, 2905 (2012)
7. M. Bello-Jiménez, C. Cuadrado-Laborde, A. Díez, J.L. Cruz, M.V. Andrés, Appl. Phys. B **105**, 269 (2011)
8. C. Cuadrado-Laborde, A. Díez, J.L. Cruz, M.V. Andrés, Appl. Phys. B **99**, 95 (2010)
9. N. Myrén, W. Margulis, IEEE Phot. Technol. Lett. **17**, 2047 (2005)
10. B.Y. kim, J.N. Blake, H.E. Engan, H.J. Shaw, Opt. Lett. **11**, 389 (1986)
11. T.A. Birks, P.St. Russell, D.O. Culverhouse et al., J. Light. Technol. **14**, 2519 (1996)
12. R. Feced, C. Alegria, M.N. Zervas, IEEE J. Select. Top. In Quant. Electron. **5**, 1278 (1999)
13. Q. Li, X. Liu, J. Peng, B. Zhou, E.R. Lyons, H.P. Lee, IEEE Phot. Technol. Lett. **14**, 337 (2002)
14. F. Abrishamian, S. Nagai, S. Sato, M. Imai, Opt. Quant. Electron. **40**, 665 (2008)
15. D.J. Kuizenga, A.E. Siegman, IEEE J. Quant. Electron. QE-6, 694 (1970)
16. Y. Li, C. Lou, M. Han, Y. Gao, Opt. Quant. Electron. **33**, 589 (2001)